Heliyon 10 (2024) e26645

Contents lists available at ScienceDirect

Heliyon

journal homepage: www.cell.com/heliyon

Research article

Feature-based 3D+t descriptors of hyperactivated human sperm beat patterns

Haydee O. Hernández [a,b], Fernando Montoya [b], Paul Hernández-Herrera [b,c], Dan S. Díaz-Guerrero [b], Jimena Olveres [d], Hermes Bloomfield-Gadêlha [e], Alberto Darszon [f], Boris Escalante-Ramírez [d], Gabriel Corkidi [b,*]

[a] Posgrado en Ciencia e Ingeniería de la Computación, Universidad Nacional Autónoma de México, UNAM, Ciudad de México, Mexico
[b] Laboratorio de Imágenes y Visión por Computadora, Instituto de Biotecnología, UNAM, Cuernavaca, Mexico
[c] Facultad de Ciencias, Universidad Autónoma de San Luis Potosí, San Luis Potosí, Mexico
[d] Departamento de Procesamiento de Señales, Facultad de Ingeniería, UNAM, Ciudad de México, Mexico
[e] Department of Engineering Mathematics and Technology, Bristol Robotics Laboratory, University of Bristol, Bristol, United Kingdom
[f] Departamento de Genética del Desarrollo y Fisiología Molecular, Instituto de Biotecnología, UNAM, Ciudad de México, Mexico

ARTICLE INFO

Keywords:
3D+t human sperm motility
Hyperactivated sperm
Sperm flagella
Spatio-temporal patterns
Unsupervised classification
Multi-plane imaging
3D microscopy

ABSTRACT

The flagellar movement of the mammalian sperm plays a crucial role in fertilization. In the female reproductive tract, human spermatozoa undergo a process called capacitation which promotes changes in their motility. Only capacitated spermatozoa may be hyperactivated and only those that transition to hyperactivated motility are capable of fertilizing the egg. Hyperactivated motility is characterized by asymmetric flagellar bends of greater amplitude and lower frequency. Historically, clinical fertilization studies have used two-dimensional analysis to classify sperm motility, despite the inherently three-dimensional (3D) nature of sperm motion. Recent research has described several 3D beating features of sperm flagella. However, the 3D motility pattern of hyperactivated spermatozoa has not yet been characterized. One of the main challenges in classifying these patterns in 3D is the lack of a ground-truth reference, as it can be difficult to visually assess differences in flagellar beat patterns. Additionally, it is worth noting that only a relatively small proportion, approximately 10-20% of sperm incubated under capacitating conditions exhibit hyperactivated motility. In this work, we used a multifocal image acquisition system that can acquire, segment, and track sperm flagella in 3D+t. We developed a feature-based vector that describes the spatio-temporal flagellar sperm motility patterns by an envelope of ellipses. The classification results obtained using our 3D feature-based descriptors can serve as potential label for future work involving deep neural networks. By using the classification results as labels, it will be possible to train a deep neural network to automatically classify spermatozoa based on their 3D flagellar beating patterns. We demonstrated the effectiveness of the descriptors by applying them to a dataset of human sperm cells and showing that they can accurately differentiate between non-hyperactivated and hyperactivated 3D motility patterns of the sperm cells. This work contributes to the understanding of 3D flagellar hyperactive motility patterns and provides a framework for research in the fields of human and animal fertility.

* Corresponding author.
E-mail address: gabriel.corkidi@ibt.unam.mx (G. Corkidi).

https://doi.org/10.1016/j.heliyon.2024.e26645
Received 24 April 2023; Received in revised form 23 November 2023; Accepted 16 February 2024

Available online 23 February 2024

1. Introduction

Human fertilization requires that sperm move and swim through the female reproductive tract to reach the egg [1–3]. This journey is accompanied by a crucial physiological process known as capacitation, involving intricate biochemical and biophysical alterations that render sperm capable of fertilization [4,5]. While sperm exhibit three-dimensional (3D) motion during this journey [6], both research and clinical analyses have predominantly been confined to capturing their movement in two-dimensional (2D) images [7–11]. Previous 2D analyses have unveiled the diverse motility patterns [12] of capacitated sperm, with one of the notable phenomena being hyperactivation. Hyperactivation is a motility pattern characterized by highly asymmetrical flagellar bends, also by an increase in amplitude and by a decrease in the frequency of beating [13–17]. Only a small percentage (around 10-20%) of the millions of ejaculated sperm are found to be capacitated after being incubated in capacitating media and consequently, exhibit non-constant hyperactivated motility [13,18]. This limited occurrence can be attributed to the asynchronous nature of the capacitating process [13,19].

It is crucial to distinguish between hyperactivation and capacitation as they represent distinct facets of sperm behavior. Capacitation refers to the functional maturation of spermatozoa, while hyperactivation refers to a specific motility pattern associated with capacitation [13]. Understanding, characterizing, and classifying hyperactivated sperm movement in 3D holds significance for male infertility diagnosis and treatment. Established methods for classifying hyperactivation motility in 2D analyses often rely on tracking sperm head trajectories, giving indirect information about the motion of the flagellum. Nevertheless, 3D flagellar hyperactivated motion has never been described.

Computer Assisted Semen Analysis (CASA) has become the gold-standard method for analyzing and classifying sperm motility in 2D. Nevertheless, it has been shown that it can produce inconsistent and subjective results as it depends largely on the expertise and training of the user [7,8]. The identification of hyperactivated human sperm used in CASA involves a combination of kinematic parameters, for sperm recorded at 60 fps: Curvilinear Velocity (VCL) $\geq$ 150 μm/s, Linearity (LIN) $\leq$ 50%, and Lateral Amplitude of Head Displacement (ALH) $\geq$ 7 μm [12]. However, these parameters may vary depending on the CASA system, frame rate and software used [8,20–22]. As an example, one subjective parameter is the ALH due to the many ways of calculating the average path. In [23], the fractal dimension (D) was proposed as an alternative to ALH. Fractal dimension indicates how much of the plane is filled by a meandering curve. If the head trajectory of a sperm's fractal dimension exceeds a threshold and satisfies the conditions for VCL and LIN, then it is considered hyperactivated.

In recent years, efforts have been made to automate and remove subjectivity from this type of analysis using machine learning and deep learning techniques [12,24–27]. However, most of these efforts have focused on analyzing sperm head trajectory and CASA parameters extracted from 2D images, leaving the analysis of 3D flagella movement largely unexplored. Recently, it has been possible to acquire images of the flagellum, for which software systems have been developed to analyze it [27–29], as is the Computer-Assisted Beat-pattern Analysis (CABA) [30]. Despite this progress, they are not capable of classifying sperm motility even in 2D. The 3D imaging and analysis of sperm flagella kinematics involves several computational challenges, including acquisition, detection, segmentation, tracking, and classification [6], but it provides more information that can help remove subjectivity in the analysis. Despite some recent progress in understanding the 3D flagellar kinematics of single sperm, the classification of 3D flagellar beating patterns in capacitated sperm remains a large gap in the literature [6,27,31–34].

Different methods have been developed to classify 3D dynamic patterns [35,36]. These include traditional machine learning techniques like decision trees and support vector machines, as well as more recent approaches based on deep learning, such as convolutional neural networks (CNNs) [37,38]. These methods rely on extensive labeled data for training, which can be a limiting factor in many cases. When labeled data are not available, unsupervised learning techniques can be employed to extract patterns or correlations from images. Unsupervised learning aims to discover inherent structures or relationships in the data without relying on prior knowledge or labeled examples. It encompasses tasks such as clustering, dimensionality reduction, and generative modeling [39,40]. In the context of classifying 3D dynamic patterns, it becomes particularly challenging to compare waveforms that change over time, such as in motion recognition or video classification [41]. The classification of 3D dynamical patterns requires a deep understanding of the temporal and spatial movement and behavior of objects, making it a complex task.

In this study, our foremost objective is to explore into the complex dynamics of sperm flagellar beating in a three-dimensional space, aiming to uncover previously unexplored patterns and characteristics of hyperactivated spermatozoa. We introduce novel descriptors for dynamic motility that are based on a set of properties displayed by ellipses enveloping the flagella, which allows to compactly describe the beating information of the flagella from 3D+t. The methodology employed in the work resulted in the identification of two distinct clusters of beating patterns through unsupervised classification. These groups were subsequently validated to distinguish between non-hyperactivated and hyperactivated entities. This validation has been accomplished by correlating these groups with established biological characteristics, such as beating amplitude, frequency, and asymmetry. Significantly, this study represents the first description of hyperactivation in 3D, laying the foundation for future 3D investigations.

2. Materials and methods

2.1. Sperm samples and media

Under informed written consent and the supervision of the Bioethics committee of the Instituto de Biotecnología, UNAM, young healthy donors supplied human spermatozoa samples by masturbation, after at least 48 hours of sexual abstinence.

The semen samples fulfilled the World Health Organization (WHO) requirements [16]. In total, there were 18 samples collected from 8 different donors. Through a swim up separation, highly motile cells were recovered from the sample that was incubated for 1 hour in Ham's F-10 medium at $37\,°C$ in a humidified chamber with a 5% CO_2 concentration. After recovery, cells were centrifuged 5 min at 3000 rpm and half of them were resuspended in a non-capacitating media and the other half in capacitating media. The non-capacitating physiological media consisted of 94 mM NaCl, 4 mM KCl, 2 mM $CaCl_2$, 1 mM $MgCl_2$, 1 mM Na pyruvate, 25 mM $NaHCO_3$, 5 mM glucose, 30 mM Hepes, and 10 mM lactate at pH 7.4. Five mg/ml of Bovine Serum Albumin (BSA) and 2 mg/ml $NaHCO_3$ were added to obtain the capacitating media.

2.2. 3D+t image acquisition

The $3D+t$ acquisition system consisted of an inverted Olympus IX71 microscope mounted on an optical table [TMC (GMP SA, Switzerland)]. A 60X water immersion objective with $N.A. = 1.00$ (Olympus UIS2 LUMPLFLN 60X W) attached to a piezoelectric device P-725 (Physik Instruments, MA, USA) mounted on the microscope. The piezoelectric along with the objective oscillated with a frequency of 90 Hz and an amplitude of 20 μm. A servo-controller E501 via a high current amplifier E-55 (Physik Instruments, MA, USA) was used to fine tune the piezoelectric oscillations. A high speed camera (NAC Q1v) with 8 GB of internal memory was set to record at 5000/8000 fps with a resolution of 640 x 480 pixels. At this speed and resolution, the camera was able to acquire 27,000 images in 5.4/3.4 seconds respectively. The acquisition system was synchronized via an E-506 function generator (NI USB-6211, National Instruments, USA). Temperature of the samples was maintained constant at $37\,°C$ with a thermal controller (Warner Instruments, TCM/CL100).

2.3. 3D waveform segmentation

The dataset consisted of 147 human spermatozoa, 60 were exposed to a non-capacitating media and 87 to capacitating media. The data were collected using the system described by Corkidi et al. [6] and the flagellum centerline was reconstructed using the segmentation process described by Hernández-Herrera et al. [32]. From the experimental conditions, it is expected that $10-20\%$ of sperm exposed to a capacitating media may display hyperactivated motility [18]. Let $(x^i_{tn}, y^i_{tn}, z^i_{tn})$, $n = 1, 2, \ldots, N_T$, be a set of points of the flagellum's centerline in a 3D coordinate system at time $t = 1, 2, \ldots, T_i$ for each spermatozoa, i, in the dataset. The number of detected flagella and points per single beat may vary over time due to the segmentation process. A complete set of these points for an experiment i in the laboratory frame of reference are shown in Fig. 1A, each colored line corresponds to a flagellum reconstruction at a given time, and the black dots represent the head of the spermatozoon. The temporal evolution is represented within the color scale shown in the figure. Every flagellum corresponds to a single temporal point and therefore each one is depicted with a single color. To place all sperm trajectories within the same comoving frame of reference, the data were both rotated and translated to align the head's main axis with the x-axis.

2.4. 3D waveform ellipse envelope

We define a flagelloid F^i_l [33] for sperm i as the set of points that belong to the flagella orthogonally projected onto the YZ plane whose x-coordinate lie in the interval $I_l = [(l-1)\cdot\delta, l\cdot\delta)$ where $l = 1, 2, \ldots, L^i$, $L^i = \lceil \frac{max\{x^i_{tn}\}}{\delta} \rceil$ (the symbols $\lceil\cdot\rceil$ denote the ceiling function, e.g., $\lceil\pi\rceil = 4$) and δ is the interval size (as shown in Fig. 1B).

$$F^i_l = \left\{ (y^i_{tn}, z^i_{tn}) | x^i_{tn} \in I_l \right\}. \tag{1}$$

Fig. 1B illustrates the fitting of an ellipse (dashed purple) to the points belonging to the flagelloid (1) using the "Direct fit of least squares of ellipses" method presented in [42]. By performing this process for each flagelloid, a set of transverse ellipses to the x-axis are obtained, which describe the motility shape of the sperm (as shown in Fig. 1C). The interval size (δ) is set to ~ 0.21 μm; this value was imposed to ensure that each interval contains at least three points. Ellipses are fitted to the flagelloid only when it has at least this number of points and they are not collinear to avoid fitting an hyperbola or a parabola (eccentricity, $\varepsilon \geq 1$). The number of ellipses $E^i | E^i \leq L^i$ are the ellipses that were fitted correctly for spermatozoon i.

From each ellipse e^i_l, we obtain four parameters:

1. The semi-major axis (a^i_l).
2. The semi-minor axis (b^i_l).
3. The angle of the ellipse (ϕ^i_l) with respect to the y-axis.
4. The eccentricity (ε^i_l).

To describe the variations in the envelope of ellipses, we propose a feature-based vector with the following four components based on an analysis of the obtained data:

- Feature 1: $\mu\left(\left\{ \sqrt{a^{i\,2}_l - b^{i\,2}_l} \right\}_{l=1}^{E^i} \right)$,

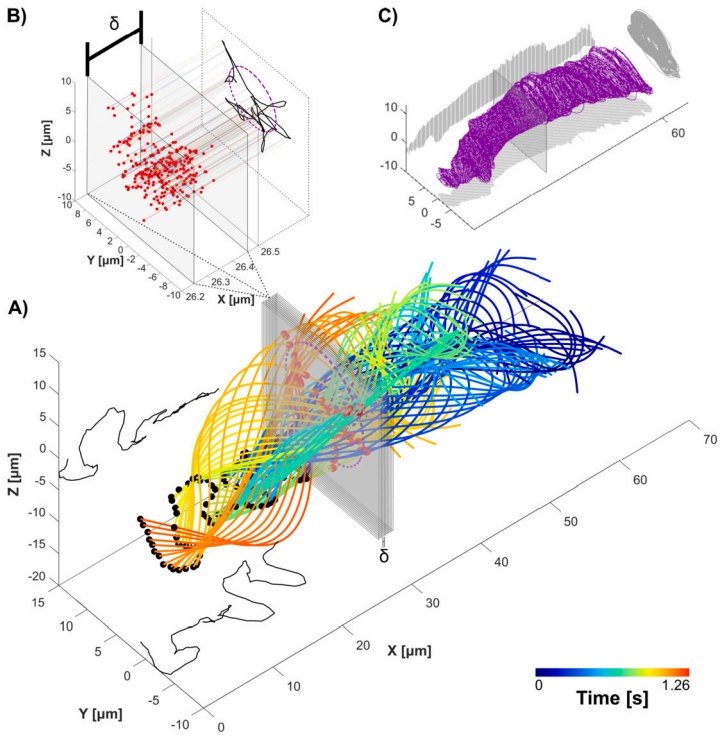

Fig. 1. A) Representation of a tracked and segmented spermatozoon, with the laboratory frame of reference data aligned along the x-axis. Each line corresponds to a flagellum reconstruction at a specific time, and the black dots represent the first point of the flagella at each time. The temporal evolution is represented within the color scale shown in the figure. Every flagellum corresponds to a single temporal point and therefore each one is depicted with a single color. The projections of the 2D head trajectories are shown in the XY and XZ planes (black lines). The process of fitting an ellipse to a flagelloid is shown with a sample out of 292 gray planes (for visualization purposes) corresponding to 10 intervals of δ each. B) Zoomed-in view of a single δ-length interval, with red dots representing the flagellum points within that interval. At the right side, the orthogonal projection of the red dots are displayed, forming a flagelloid (black line) and its fitted ellipse (purple dotted line). C) Envelope of ellipses (purple lines) and their XY, XZ, and YZ projections (light gray lines) for a spermatozoon. Each ellipse was fitted to an interval, the complete envelope is composed with all the ellipses fitted to the sperm's beating.

Table 1
Detailed table of the principal component analysis.

	PC 1	PC 2	PC 3
Eigenvalue	2.3862	1.0004	0.4616
Feature 1	**0.6142**	0.0392	-0.1122
Feature 2	-0.0242	**0.9990**	-0.0191
Feature 3	0.5712	-0.0163	-0.6197
Feature 4	0.5440	0.0172	**0.7765**

Details of the principal component analysis obtained from the feature-based vector of the envelope of ellipses. The element $[j,k]$ is the contribution of the Feature j to the k-th PC. The dominant features for each principal component are shown in bold.

- Feature 2: $\mu\left(\left\{\phi_{l-1}^{i}-\phi_{l}^{i}\right\}_{l=2}^{E^i}\right)$,
- Feature 3: $\mu\left(\left\{\epsilon_{l}^{i}\right\}_{l=1}^{E^i}\right)$,
- Feature 4: $\sigma\left(\left\{a_{l}^{i}\right\}_{l=1}^{E^i}\right)$,

where μ is the average and σ is the standard deviation. Feature 1 is the average distance from the center of the ellipse to the focus of every ellipse, Feature 2 is the average of the difference between angles of the major axis of consecutive ellipses, Feature 3 is the average value of the eccentricity and Feature 4 is the standard deviation of the semi-major axis. Then we reduce the dimensionality of the vector using Principal Component Analysis (PCA), resulting in three principal components that account for more than 90% of the variance in the dataset (see Table 1).

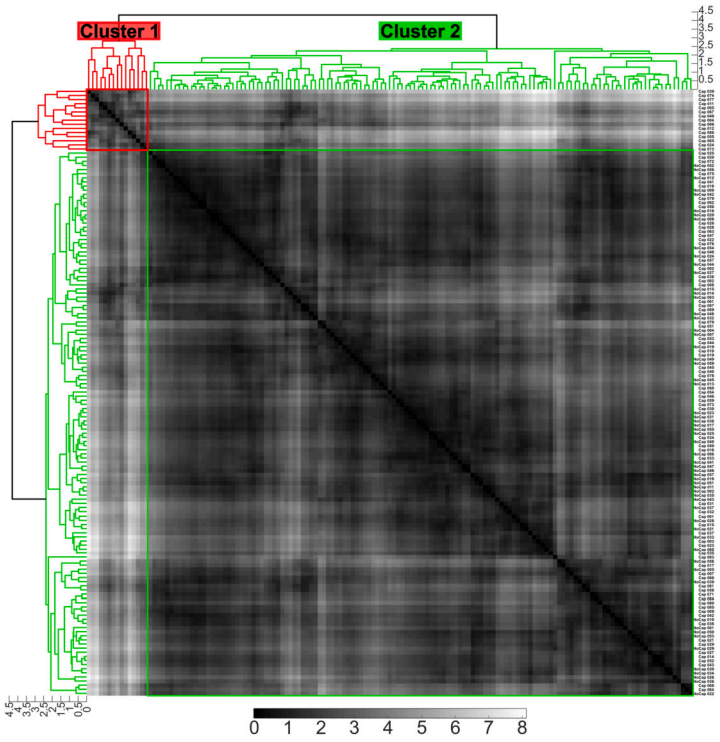

Fig. 2. The dissimilarity matrix shows the Euclidean distance between each pair of sperm cells based on their four principal components. The pixel intensity in the matrix corresponds to the distance value. On the right, the IDs of each experiment are displayed, where "No Cap" belongs to the control group and "Cap" refers to the spermatozoa exposed to capacitating conditions. The dendrogram shows the hierarchical clustering with average linkage; red lines correspond to Cluster 1 and green lines to Cluster 2.

2.5. Clustering

Our dataset consists of samples incubated in non-capacitated media (control) and sperm that have been incubated under capacitating conditions, we expect that around 10 - 20% of the capacitated sperm at most, will exhibit an hyperactivated motility pattern. Since our dataset cannot be labeled, we did not have prior knowledge of the number of clusters in the data, and the actual number of hyperactivated sperm cells is unknown. We choose to apply agglomerative hierarchical clustering, since it does not require knowing a priori how many clusters there are, does not need input parameters, and is less sensitive to outliers compared to other methods. Agglomerative hierarchical clustering [43] is a technique that clusters each of the objects in the dataset based on the dissimilarity metric between them. The clusters are created between pairs of greater similarity and then, they are successively connected with the other pairs of less similarity. This process is represented through a dendrogram that shows the hierarchical relationship between group-pairs in the dataset [43]. We used the Euclidean distance as the dissimilarity metric between the descriptors of each sperm cell with all the others to determine the dissimilarity between each pair of spermatozoa. We used average linkage and "distance" as the criterion to define the clusters based on proximity between the objects. The dendrogram enabled us to visually identify the number of main groups in the dataset, and we identified two main clusters.

3. Results

The dissimilarity matrix of the Euclidean distance between each pair of spermatozoa is depicted in Fig. 2, illustrating how similar they are based on their feature-based descriptors. The diagonal of the matrix is black since a feature-based descriptor's distance from itself is 0 (high similarity), while pairs of sperm with higher distances are represented with white (low similarity). The cells that were incubated under non-capacitating conditions and a fraction of the incubated under capacitating conditions sperm are found in Cluster 2 (green square and lines in Fig. 2). Spermatozoa in Cluster 1 (red squares and lines in Fig. 2) have fitted ellipses with semi-major axes that are larger ($max(a) > 6.5$ μm) than those in cluster 2 in addition to having $\varepsilon \to 1$. The ellipse's eccentricity (ε) measures how much it deviates from a circle. This is related to the tendency of the flagellum's beating pattern, with a more isotropic pattern corresponding to a more circular ellipse ($\varepsilon \to 0$) and an anisotropic pattern corresponding to a more elongated ellipse ($\varepsilon \to 1$). Given the previous analysis and considerations, we associate Cluster 2 to the motility pattern of non-hyperactivated sperm, which includes the control group and a subset of spermatozoa incubated under capacitating conditions (those exposed to a capacitating media, not showing hyperactivated motility), as shown in the next validating section. Cluster 1 is then associated with the hyperactivated beating pattern group, which only includes sperm cells that were exposed to capacitating conditions.

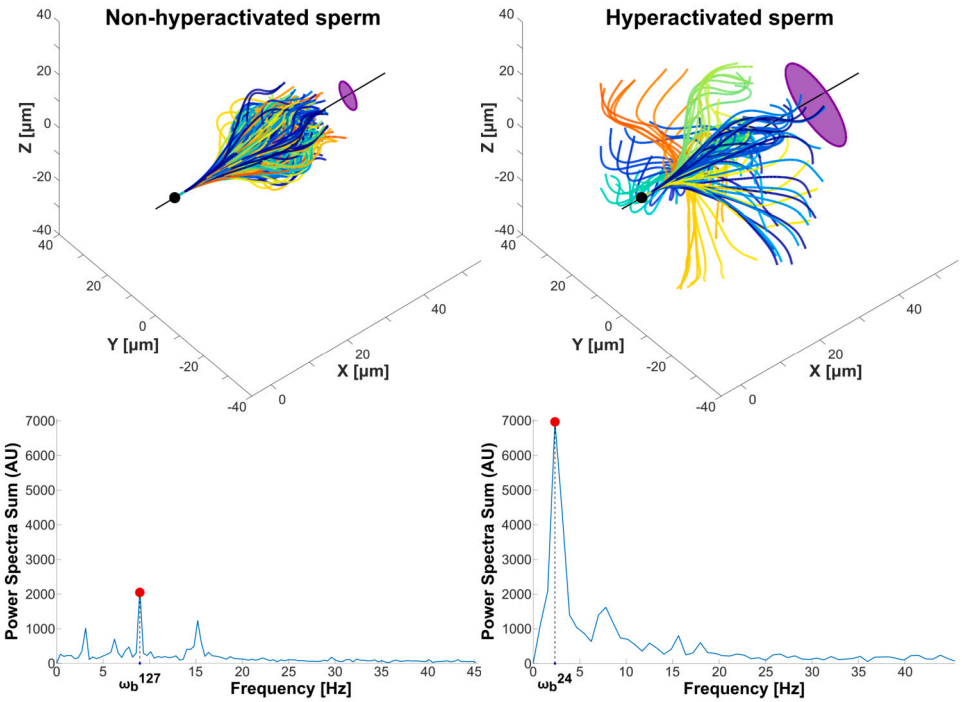

Fig. 3. The upper graphs show the flagellar beat of a sperm classified as non-hyperactivated (left side) and one classified as hyperactivated (right side). Both are aligned and rotated with respect to the x-axis (black line) along the first ~ 2.5 μm of arclength, corresponding to the mid-head of the sperm. The ellipse at the end of the x-axis shows the average ellipse fitted to the flagellar beat, indicating the average anisotropy of the beat. The lower graphs, as instances of the examples in the upper ones, display the sum of the amplitude spectrum of all points. The red dots on these plots represent the maximum value of the spectrum, associated with the sperm beat frequency, ω_b^i.

3.1. Validating the classification of the 3D sperm beating patterns

In the literature, it has been described that hyperactivated motility in human spermatozoa is characterized by asymmetric flagellar beating, an increase in amplitude, and a decrease in the frequency of beating [1,14,18,20,44–46]. To validate our unsupervised classification of motility patterns, we have measured these features (amplitude, frequency, and asymmetry) in 3D+t from our database and proposed some 3D generalizations of the 2D well-known measures. For this purpose, the first ~ 2.5 μm of arclength of each flagellum was aligned and rotated with respect to the x-axis (see Fig. 3).

For each individual sperm (denoted as i), we defined the amplitude as the average distance of each point on the flagellum (represented by coordinates $(x_{tn}^i, y_{tn}^i, z_{tn}^i)$) to the x-axis:

$$A^i = \mu\left(\left\{\sqrt{{y_{tn}^i}^2 + {z_{tn}^i}^2}\right\}_{n=1,t=1}^{N_T,T_i}\right). \tag{2}$$

The beat frequency is obtained through the analysis of the Fourier transform on each point of the flagellum over the time $\mathcal{F}(y_{tn}^i,\ z_{tn}^i)$. The power spectrum amplitude of each point of the sum of the two components are summed and the frequency with peak amplitude is taken as the maximum frequency (Fig. 3):

$$\omega_b^i = argmax_\omega\left(\sum_{n=1}^{N}|\mathcal{F}\{y_{tn}^i\}| + |\mathcal{F}\{z_{tn}^i\}|\right). \tag{3}$$

While the increase in asymmetry for hyperactivated spermatozoa is clearly observable in 2D analysis, it becomes more challenging to measure and generalize this asymmetry directly in 3D data. However, an alternative approach in the 3D context is to consider anisotropy. The anisotropy is taken as the mean of the eccentricity of the ellipses fitted to each spermatozoon. Anisotropy captures the directional preference or orientation of the envelope of ellipses in 3D, providing valuable insights into the movement patterns of hyperactivated spermatozoa. In the context of measuring the eccentricity of the envelope of ellipses in sperm flagellar beat analysis, a higher eccentricity value indicates a more elongated or stretched shape, which implies a higher anisotropy of the beat. This means that the flagellum exhibits a preferred direction or orientation of bending, leading to an elongated shape rather than a circular shape.

We performed the Wilcoxon Rank Sum Test to determine if there were differences between the two clusters for each measure described above (Fig. 4), this test is used when the sizes of the samples are relatively small and they are not normally distributed, showing a significant difference.

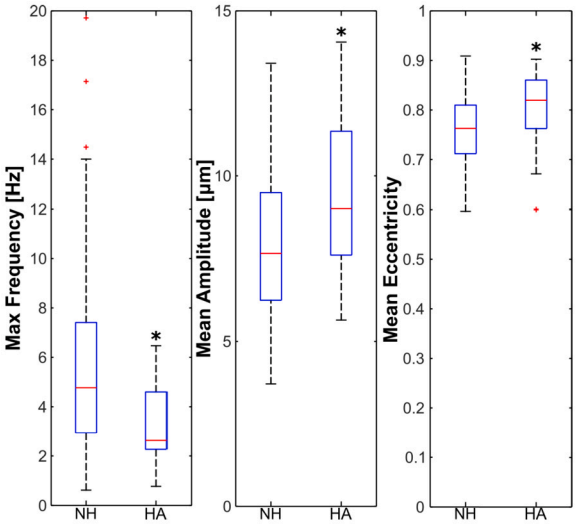

Fig. 4. Boxplots of the frequency, amplitude, and, anisotropy values for each motility group identified (non-hyperactivated: NH, and hyperactivated: HA). The *p*-value for the Wilcoxon test for each feature is: 0.009, 0.01 and 0.0476 respectively $^{*}P < 0.05$.

4. Discussion

This work introduces a feature-based vector that captures the average dynamics of the flagellar beat in 3D+t. Leveraging these descriptors, we successfully achieved the unsupervised classification of human spermatozoa flagellar beating into non-hyperactivated and hyperactivated classes. Notably, this unsupervised approach circumvents the need for labeled training data and offers a robust methodology.

In the context of sperm motility analysis, previous studies have observed that hyperactivated spermatozoa exhibit an asymmetrical beating pattern compared to non-hyperactivated ones [17]. Building upon this observation, our proposed envelope of ellipses allows the generalization of this description to the 3D case. This simplifies 3D movement to a surface that fits the flagellar beat. Here we test the hypothesis that the shape of this envelope is correlated with the waveform of sperm non-hyperactivated and hyperactivated states. Ellipses with eccentricities close to one correspond to elongated shapes, indicative of an anisotropic envelope, while ellipses with eccentricities close to zero represent more symmetrical envelopes. Moreover, this characterization enables the quantification of the 3D equivalent of the movement envelope amplitude through the descriptor of the foci average of the ellipses. Significantly, the amplitude feature is found to be smaller for the non-hyperactivated group compared to the hyperactivated group.

In addition to capturing anisotropy and amplitude of the envelope, the proposed feature-based vector provides a parameter-free representation of flagellar beat dynamics, allowing an objective classification. By using this approach, we accurately classified the entire set of the exposed to a non-capacitating media sperm, along with the non-hyperactivated sperm from the incubated under capacitating conditions group, into the green cluster (Fig. 2). As we expected, approximately 17% of the incubated under capacitating conditions spermatozoa belong to the hyperactivated group, as mentioned in [18].

Given the absence of a ground truth for 3D classification, we initially compared the unsupervised classification results using the most common 2D characteristics of hyperactivated motility: frequency and amplitude, measured in 3D. However, measuring asymmetry in a 3D context is not straightforward. Asymmetry in the flagellar beat refers to the differences or variations between the two sides or halves of the flagellum. Instead, in this study, we utilized the eccentricity as a measure of anisotropy, which captures the preferred direction of the beat's envelopes. While eccentricity primarily quantifies anisotropy rather than direct asymmetry, it can still provide valuable insights into the beat patterns. Higher eccentricity values indicate a more elongated shape of the beat, suggesting a higher degree of anisotropy. This measure of anisotropy serves as an indirect measure of the asymmetry of the flagellar beat. Through these comparisons, we observed that the hyperactivated group exhibited lower frequency, higher mean amplitude, and greater anisotropy of the waveform path compared to the non-hyperactivated group. These findings suggest that these 2D characteristics, along with the measure of anisotropy, can serve as informative features in distinguishing between non-hyperactivated and hyperactivated spermatozoa. The Wilcoxon test confirmed that the two groups were statistically different in terms of each attribute (frequency, amplitude, and anisotropy).

Alternative measurements to describe the motility patterns of the cell have been explored. One relevant example is the fractal dimension of the 2D trajectory of the cell head. It has been shown that 2D trajectories with a fractal dimension greater than 1.3 could be an hyperactivated motility pattern [23]. How this 2D head trajectory measurement could be correlated to our present 3D flagellar approach surges as a research venue.

The findings presented in this work align with our previous studies [47], further substantiating the reliability of our feature-based descriptors in characterizing motility patterns. To enhance the accuracy and validation of these results, future work will involve using fluorescent markers to establish a ground truth reference for hyperactivated human sperm in 3D.

5. Conclusions

This study addresses the critical need for describing the 3D flagellar beating patterns of human spermatozoa and presents a reliable and simple classification framework. By overcoming the limitations of subjective expert-based analysis, our approach offers a robust means of characterizing motility patterns.

The unique contribution of this work lies in the development of a robust classification methodology that does not rely on deep neural networks. This is particularly significant because deep learning approaches are not viable due to the lack of labeled 3D+t beating data. Furthermore, by simplifying the intricate spatio-temporal data in three dimensions, we transform each flagellum point, which essentially represents a time series, into a shape analysis that considers both the flagellum's shape and the accumulated movement of the sperm in 3D through the waving movement envelope. The classification results obtained using our feature-based descriptors can serve as potential labels for future work involving deep neural networks. By using the classification results as labels, it will be possible to train a deep neural network to automatically classify spermatozoa based on their flagellar beating patterns. This combination of feature-based descriptors and deep neural networks holds promise for further improving the accuracy and efficiency of classification tasks in reproductive biology and fertility research.

Funding

This work was supported by Dirección General de Asuntos del Personal Académico, Universidad Nacional Autónoma de México (UNAM-PAPIIT) under the Grant TA101121, Grant IV100420, Grant IN204922 and Grant IN105222. Paul Hernández-Herrera was supported by the Chan Zuckerberg Initiative DAF under the Grant 2023-329644. Dan S. Díaz-Guerrero was supported by a Postdoctoral fellowship from Consejo Nacional de Humanidades, Ciencias y Tecnologías, CONAHCYT–México CVU 289856 and the work of Haydee O. Hernández was supported by a Ph.D. scholarship from CONAHCYT–México CVU 700563.

Compliance with ethical standards

This work was approved by the Bioethics Committee permit for project IN200919. Signed written informed consent forms were signed by all healthy donors.

CRediT authorship contribution statement

Haydee O. Hernández: Conceptualization, Data curation, Formal analysis, Investigation, Methodology, Software, Validation, Visualization, Writing – original draft, Writing – review & editing. **Fernando Montoya:** Conceptualization, Data curation, Formal analysis, Investigation, Methodology, Software, Supervision, Validation, Visualization, Writing – original draft, Writing – review & editing. **Paul Hernández-Herrera:** Data curation, Investigation, Methodology, Software, Visualization, Writing – original draft, Writing – review & editing. **Dan S. Díaz-Guerrero:** Data curation, Formal analysis, Investigation, Methodology, Software, Validation, Writing – original draft, Writing – review & editing. **Jimena Olveres:** Investigation, Supervision, Validation, Writing – original draft, Writing – review & editing. **Hermes Bloomfield-Gadêlha:** Formal analysis, Investigation, Methodology, Supervision, Validation, Writing – original draft, Writing – review & editing. **Alberto Darszon:** Conceptualization, Formal analysis, Funding acquisition, Investigation, Methodology, Project administration, Resources, Supervision, Validation, Writing – original draft, Writing – review & editing. **Boris Escalante-Ramírez:** Conceptualization, Formal analysis, Funding acquisition, Investigation, Methodology, Project administration, Resources, Software, Supervision, Validation, Writing – original draft, Writing – review & editing. **Gabriel Corkidi:** Conceptualization, Data curation, Formal analysis, Funding acquisition, Investigation, Methodology, Project administration, Resources, Supervision, Validation, Visualization, Writing – original draft, Writing – review & editing.

Declaration of competing interest

The authors declare that they have no known competing financial interests or personal relationships that could have appeared to influence the work reported in this paper.

Data availability

The data underlying this article will be shared upon reasonable request to the corresponding author.

Declaration of generative AI and AI-assisted technologies in the writing process

During the preparation of this work the authors used ChatGPT in order to assist in refining the language. After using this tool, the authors reviewed and edited the content as needed and take full responsibility for the content of the publication.

References

[1] S.S. Suarez, A. Pacey, Sperm transport in the female reproductive tract, Hum. Reprod. Updat. 12 (1) (2006) 23–37.

[2] M.J. Freitas, S. Vijayaraghavan, M. Fardilha, Signaling mechanisms in mammalian sperm motility, Biol. Reprod. 96 (1) (2017) 2–12.
[3] E.A. Gaffney, H. Gadêlha, D.J. Smith, J.R. Blake, J.C. Kirkman-Brown, Mammalian sperm motility: observation and theory, Annu. Rev. Fluid Mech. 43 (2011) 501–528.
[4] R. Yanagimachi, Mammalian sperm acrosome reaction: where does it begin before fertilization?, Biol. Reprod. 85 (1) (2011) 4–5.
[5] G. Corkidi, P. Hernández-Herrera, F. Montoya, H. Gadêlha, A. Darszon, Long-term segmentation-free assessment of head–flagellum movement and intracellular calcium in swimming human sperm, J. Cell Sci. 134 (3) (2021) jcs250654.
[6] G. Corkidi, B. Taboada, C. Wood, A. Guerrero, A. Darszon, Tracking sperm in three-dimensions, Biochem. Biophys. Res. Commun. 373 (1) (2008) 125–129.
[7] S.T. Mortimer, G. Van der Horst, D. Mortimer, The future of computer-aided sperm analysis, Asian J. Androl. 17 (4) (2015) 545.
[8] D. Bompart, A. García-Molina, A. Valverde, C. Caldeira, J. Yániz, M.N. de Murga, C. Soler, Casa-mot technology: how results are affected by the frame rate and counting chamber, Reprod. Fertil. Dev. 30 (6) (2018) 810–819.
[9] C. Alquézar-Baeta, S. Gimeno-Martos, S. Miguel-Jiménez, P. Santolaria, J. Yániz, I. Palacín, A. Casao, J.Á. Cebrián-Pérez, T. Muiño-Blanco, R. Pérez-Pé, Opencasa: a new open-source and scalable tool for sperm quality analysis, PLoS Comput. Biol. 15 (1) (2019) e1006691.
[10] R. Dcunha, R.S. Hussein, H. Ananda, S. Kumari, S.K. Adiga, N. Kannan, Y. Zhao, G. Kalthur, Current insights and latest updates in sperm motility and associated applications in assisted reproduction, Reprod. Sci. (2020) 1–19.
[11] J.-w. Choi, L. Alkhoury, L.F. Urbano, P. Masson, M. VerMilyea, M. Kam, An assessment tool for computer-assisted semen analysis (casa) algorithms, Sci. Rep. 12 (1) (2022) 16830.
[12] S.G. Goodson, S. White, A.M. Stevans, S. Bhat, C.-Y. Kao, S. Jaworski, T.R. Marlowe, M. Kohlmeier, L. McMillan, S.H. Zeisel, et al., Casanova: a multiclass support vector machine model for the classification of human sperm motility patterns, Biol. Reprod. 97 (5) (2017) 698–708.
[13] A. Cohen-Dayag, I. Tur-Kaspa, J. Dor, S. Mashiach, M. Eisenbach, Sperm capacitation in humans is transient and correlates with chemotactic responsiveness to follicular factors, Proc. Natl. Acad. Sci. 92 (24) (1995) 11039–11043.
[14] N. Sukcharoen, J. Keith, D.S. Irvine, R.J. Aitken, Definition of the optimal criteria for identifying hyperactivated human spermatozoa at 25 hz using in-vitro fertilization as a functional end-point, Hum. Reprod. 10 (11) (1995) 2928–2937.
[15] H. Chang, S.S. Suarez, Two distinct ca2+ signaling pathways modulate sperm flagellar beating patterns in mice, Biol. Reprod. 85 (2) (2011) 296–305.
[16] W.H. Organization, et al., WHO Laboratory Manual for the Examination and Processing of Human Semen, World Health Organization, 2021.
[17] D. Waberski, S.S. Suarez, H. Henning, Assessment of sperm motility in livestock: perspectives based on sperm swimming conditions in vivo, Anim. Reprod. Sci. 246 (2022) 106849.
[18] S.S. Suarez, Control of hyperactivation in sperm, Hum. Reprod. Updat. 14 (6) (2008) 647–657.
[19] S. Pérez-Cerezales, S. Boryshpolets, M. Eisenbach, Behavioral mechanisms of mammalian sperm guidance, Asian J. Androl. 17 (4) (2015) 628.
[20] V. Kay, L. Robertson, Hyperactivated motility of human spermatozoa: a review of physiological function and application in assisted reproduction, Hum. Reprod. Updat. 4 (6) (1998) 776–786.
[21] S.T. Mortimer, A critical review of the physiological importance and analysis of sperm movement in mammals, Hum. Reprod. Updat. 3 (5) (1997) 403–439.
[22] C. Castellini, A. Dal Bosco, S. Ruggeri, G. Collodel, What is the best frame rate for evaluation of sperm motility in different species by computer-assisted sperm analysis?, Fertil. Steril. 96 (1) (2011) 24–27.
[23] S.T. Mortimer, M.A. Swan, D. Mortimer, Fractal analysis of capacitating human spermatozoa, Hum. Reprod. 11 (5) (1996) 1049–1054.
[24] S. Javadi, S.A. Mirroshandel, A novel deep learning method for automatic assessment of human sperm images, Comput. Biol. Med. 109 (2019) 182–194.
[25] P.Â.P. da Silva, Supervised and Unsupervised Spermatozoa Detection, Classification and Tracking in Imaging Data, PhD thesis, Universidade de Lisboa, Portugal, 2011.
[26] J. Riordon, C. McCallum, D. Sinton, Deep learning for the classification of human sperm, Comput. Biol. Med. 111 (2019) 103342.
[27] J.B. You, C. McCallum, Y. Wang, J. Riordon, R. Nosrati, D. Sinton, Machine learning for sperm selection, Nat. Rev. Neurol. 18 (7) (2021) 387–403.
[28] J.N. Hansen, S. Rassmann, J.F. Jikeli, D. Wachten, Spermq–a simple analysis software to comprehensively study flagellar beating and sperm steering, Cells 8 (1) (2018) 10.
[29] M.T. Gallagher, G. Cupples, E.H. Ooi, J. Kirkman-Brown, D. Smith, Rapid sperm capture: high-throughput flagellar waveform analysis, Hum. Reprod. 34 (7) (2019) 1173–1185.
[30] B.J. Walker, S. Phuyal, K. Ishimoto, C.-K. Tung, E.A. Gaffney, Computer-assisted beat-pattern analysis and the flagellar waveforms of bovine spermatozoa, R. Soc. Open Sci. 7 (6) (2020) 200769.
[31] G. Corkidi, F. Montoya, P. Hernández-Herrera, W. Ríos-Herrera, M. Müller, C. Treviño, A. Darszon, Are there intracellular ca2+ oscillations correlated with flagellar beating in human sperm? A three vs. two-dimensional analysis, Mol. Hum. Reprod. 23 (9) (2017) 583–593.
[32] P. Hernandez-Herrera, F. Montoya, J.M. Rendón-Mancha, A. Darszon, G. Corkidi, 3-d $+t$ human sperm flagellum tracing in low snr fluorescence images, IEEE Trans. Med. Imaging 37 (10) (2018) 2236–2247.
[33] H. Gadêlha, P. Hernández-Herrera, F. Montoya, A. Darszon, G. Corkidi, Human sperm uses asymmetric and anisotropic flagellar controls to regulate swimming symmetry and cell steering, Sci. Adv. 6 (31) (2020) eaba5168.
[34] A. Gong, S. Rode, G. Gompper, U.B. Kaupp, J. Elgeti, B. Friedrich, L. Alvarez, Reconstruction of the three-dimensional beat pattern underlying swimming behaviors of sperm, Eur. Phys. J. E 44 (7) (2021) 87.
[35] A. Danelakis, T. Theoharis, I. Pratikakis, P. Perakis, An effective methodology for dynamic 3d facial expression retrieval, Pattern Recognit. 52 (2016) 174–185.
[36] M. Körtgen, G.-J. Park, M. Novotni, R. Klein, 3d shape matching with 3d shape contexts, in: The 7th Central European Seminar on Computer Graphics, vol. 3, Budmerice Slovakia, 2003, pp. 5–17.
[37] H.-C. Shin, H.R. Roth, M. Gao, L. Lu, Z. Xu, I. Nogues, J. Yao, D. Mollura, R.M. Summers, Deep convolutional neural networks for computer-aided detection: Cnn architectures, dataset characteristics and transfer learning, IEEE Trans. Med. Imaging 35 (5) (2016) 1285–1298.
[38] Z. Che, S. Purushotham, K. Cho, D. Sontag, Y. Liu, Recurrent neural networks for multivariate time series with missing values, Sci. Rep. 8 (1) (2018) 6085.
[39] Z. Ghahramani, Unsupervised learning, in: Advanced Lectures on Machine Learning: ML Summer Schools 2003, Canberra, Australia, February 2-14, 2003, Tübingen, Germany, August 4-16, 2003, Revised Lectures, 2004, pp. 72–112.
[40] S. Badillo, B. Banfai, F. Birzele, I.I. Davydov, L. Hutchinson, T. Kam-Thong, J. Siebourg-Polster, B. Steiert, J.D. Zhang, An introduction to machine learning, Clin. Pharmacol. Ther. 107 (4) (2020) 871–885.
[41] P. Huang, J. Starck, A. Hilton, Temporal 3d shape matching, in: 4th European Conference on Visual Media Production, IET, 2007, pp. 1–10.
[42] E.S. Maini, Enhanced direct least square fitting of ellipses, Int. J. Pattern Recognit. Artif. Intell. 20 (06) (2006) 939–953.
[43] A.K. Jain, R.C. Dubes, Algorithms for Clustering Data, Prentice-Hall, Inc., 1988.
[44] E. De Lamirande, P. Leclerc, C. Gagnon, Capacitation as a regulatory event that primes spermatozoa for the acrosome reaction and fertilization, Mol. Hum. Reprod. 3 (3) (1997) 175–194.
[45] M. Zaferani, S.S. Suarez, A. Abbaspourrad, Mammalian sperm hyperactivation regulates navigation via physical boundaries and promotes pseudo-Chemotaxis, Proc. Natl. Acad. Sci. 118 (44) (2021) e2107500118.
[46] A. Agarwal, G. Virk, C. Ong, S.S. Du Plessis, Effect of oxidative stress on male reproduction, World J. Men's Health 32 (1) (2014) 1–17.
[47] H.O. Hernández, P. Hernández-Herrera, F. Montoya, J. Olveres, H. Bloomfield-Gadêlha, A. Darszon, B. Escalante-Ramírez, G. Corkidi, 3d+ t feature-based descriptor for unsupervised flagellar human sperm beat classification, in: 2022 44th Annual International Conference of the IEEE Engineering in Medicine & Biology Society (EMBC), IEEE, 2022, pp. 488–492.